CCAT-prime: 'Multi-map' Holographic Measurement for the FYST Testbed – Near-field beam measurement and Data analysis

Xiaodong Ren[1], Urs U. Graf[1], Pablo Astudillo[2], Sebastian Jorquera[2], Richard E. Hills[3], Bojan Nikolic[3], Stephen C. Parshley[4], Nicolás Reyes[5], Lars Weikert[1] and Jürgen Stutzki[1]

***Abstract*—A novel method based on microwave holography has been developed to align the optics of the Fred Young Sub-millimeter Telescope (FYST). The telescope uses a crossed-Dragone configuration with a 6 meters primary dish and a similar size sub-reflector. To reach high efficiency in the sub-millimeter band, it requires a surface precision better than 10.7 µm. The proposed method requires measuring four or more beam maps by putting the receiver at different points in the focal plane to break the phase degeneracy between the reflectors. Therefore, we refer to this method as 'Multi-map' holography. The system is designed to operate at around 300GHz to achieve a measurement accuracy better than 2 µm. In this report, a small model of the FYST has been constructed to demonstrate the feasibility of this new holography metrology in the laboratory. Conventional one-beam holography and the new 'Multi-map' measuring were carried out to measure the artificial surface errors on the reflectors of the small telescope. The results prove that the errors on the two reflectors can be discriminated and measured with a statistic error lower than 1 µm. The measurement also indicates that the large spatial errors existing on the two reflectors also can be observed.**

***Index Terms*—microwave, holography, alignment, sub-millimeter telescope, crossed-Dragone, CCAT-prime.**

I. Introduction

MEASURING and correcting the surface deformation of large radio telescopes are critical to preserving the electromagnetic performance of the telescope at the highest operating frequency. One conventional surface diagnosis method is microwave holography [1] [2], which directly measures the telescope's beam in both amplitude and phase and converts the beam to the complex fields on the reflector surface. Then the offset of the reflector from its original position can be computed by using the phase term of the solved surface fields. This technique is regularly used at almost all sub-millimeter telescopes around the world, and offers an efficient and accurate way for adjusting the reflectors. But It is always used in conventional telescopes where only one large reflector needs to be adjusted. For systems having two reflectors, e.g., the crossed-Dragone optics [3] [4] used in the FYST [5] [6], employing this method only indicates that reflector deformations exist, but cannot identify which of the two mirrors is deformed, i.e., it cannot resolve the surface error degeneracy in the two-mirror system. A new method, which measures several beams with the receiver placed in different well-separated points in the focal plane, was proposed for the FYST telescope in paper [7]. In this report, a 1/15$^{\text{th}}$-scale model of the FYST was constructed as a testbed to demonstrate the feasibility of the new proposed method.

[1]I. Physikalisches Institut, Universität zu Köln,Germany; [2]Departamento de Astronomía, Universidad de Chile,Chile; [3]Cavendish Laboratory, University of Cambridge, UK; [4]Department of Astronomy, Cornell University, USA; [5]Max Planck Institute for Radio Astronomy, Germany.

II. LABORATORY HOLOGRAPHY DESIGN

The FYST reflectors are built using 146 rectangular panels, 77 on the primary mirror and 69 on the secondary, with panel sizes of 670 × 750 mm and 700 × 710 mm respectively. We would use a spatial resolution of 10×10 cm^2 to properly solve the panel deformations on the measured surface error maps. Translating this requirement to the laboratory model indicates that a spatial resolution of 10×10 mm^2 is reasonable for the 400mm diameter laboratory antenna. This means a 5.7×5.7 deg^2 beam map extension needs to be measured at 300GHz. The technical details of the holographic design of the scale model and the full FYST system are compared and summarized in Table I. The laboratory setup is illustrated in Fig. 1. The Antenna and transmitter are separated by ∼5 meters, and the beams are measured by scanning the transmitter that is moved by an XY-scanner. The reference receiver is mounted beside the antenna, 275mm from the primary reflector (M1) center. The pathlength from the transmitter to the reference receiver is not fixed. The phase modifications on the observed beam by the pathlength changes have to be corrected by geometrical optics.

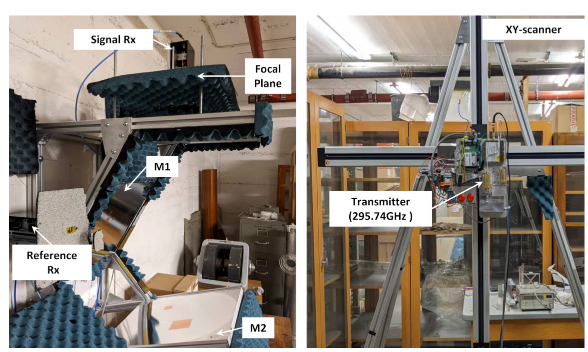

Fig. 1. Laboratory holographic testbed. Left: the 1/15$^{\text{th}}$-scale FYST telescope, 400mm in diameter, and the location of the signal and reference receiver; right: the transmitter mounted on an XY-scanner is located at ∼5 meters away from the antenna to illuminate the telescope. The scanner can move in the range of ±550mm along x and y directions.

TABLE I
CRITICAL HOLOGRAPHIC DESIGN

	Lab	**FYST**
Operating Wavelength (λ):	1.0137mm	1.0137mm
Telescope Aperture:	400mm	6000mm
Distance from source to antenna:	5m	300m
New focus (behind nominal focus):	200mm	705mm
Accuracy:	$< 2\,\mu$m	$< 2\,\mu$m
Spatial Resolution:	10mm	100mm
Required angular range:	$5.7°$	$0.57°$
Source scan range:	$\pm 250mm$	$\pm 1500mm$
S/N:	>64dB	>67dB
Number of field points	51×51	(71×71)
Receiver position spacing:	100mm	800mm

The two receivers and transmitter adopt the same diagonal horn [8] whose half-power beamwidth is about 16 degrees. The extra optics designed for reference receiver and transmitter modules in the original FYST holography [7] is removed because of the laboratory setup's shorter distance and broader beam map size requirement.

The beam maps of the Lab antenna are measured by placing the signal receiver to 5 points in the focal plane, at the center and the four corners of a square with side length of 100mm, see Fig. 2. Since the source is around 5 meters away from the telescope, to refocus the optics the receiver is moved back 200mm from the astronomical focus.

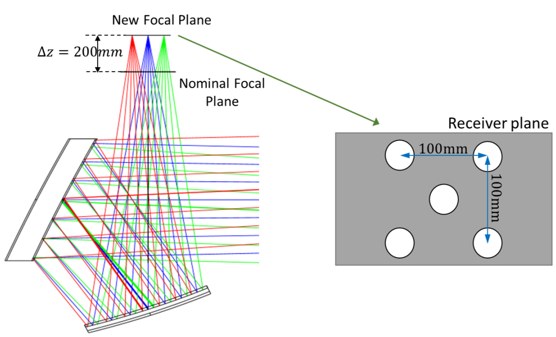

Fig. 2. Optical layout of the laboratory antenna (left). 5 receiver positions in the receiver plane (right).

III. BEAM MEASUREMENT AND ANALYSIS

The beams are measured by scanning the transmitter column by column with a constant speed. The field points are recorded using a digital cross-correlation spectrometer with ~100Hz sampling rate (~10ms integration time). The recorded data and position of field points are synchronized by time stamp. To calibrate the effect of systematic drift, the transmitter is moved to the beam center every 20s. After the beam scan, the impact of the phase and amplitude structure of the reference receiver beam needs to be removed from the recorded data.

To check the feasibility and accuracy of the holographic system, a copper foil with a thickness of $50\,\mu$m is used to create artificial piston errors on the mirror surfaces, and plastic tapes are applied to produce equivalent piston error in the opposite direction. Fig. 3 shows the artificial error patches on the mirrors. Then the one-beam holography and multi-map analysis are both measured to diagnose the antenna optics.

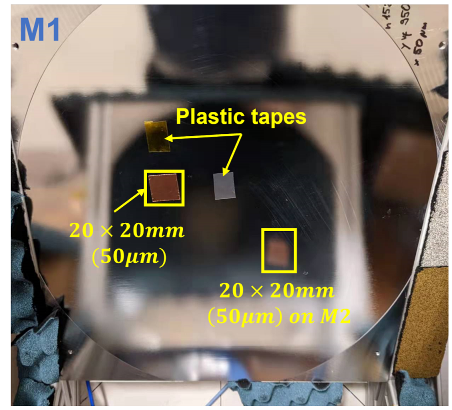

Fig. 3. Artificial piston errors on M1 and M2 made by copper foils and plastic tapes.

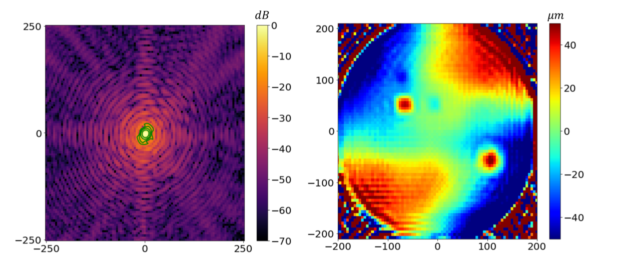

Fig. 4. Conventional one-beam holographic analysis. Left: the measured focused central beam; Right: equivalent surface deformations at the surface of M1.

A. Conventional One-beam Holography

The conventional holography just measures the focused beam with the receiver mounted in the center of the focal plane, see Fig. 4 (left). Since the beam is measured in the source plane that is parallel to the aperture plane of the antenna, we can convert the beam map labelled by $f_A(x, y)$ to the aperture fields expressed by $f_B(x, y)$ using technique of physical optics propagation [10]. data analysis processes are summarized below:

1) Calculate angular spectrum $F_A(u, v)$ of the observed fields using fast Fourier transform, where u and v are expressed by $\sin\theta \cdot \cos\phi$ and $\sin\theta \cdot \sin\phi$ respectively. θ and ϕ represent the elevation and azimuth angles.
2) Compute the angular spectrum of the field in aperture $F_B(u, v)$ using physical optics propagation technique expressed by the formula of $F_B = F_A \cdot exp(j\frac{2\pi}{\lambda}\Delta z \cdot \sqrt{1 - u^2 - v^2})$, where Δz is the distance between field planes.
3) Make inverse Fourier transform on the new angular spectrum $F_B(u, v)$ to get the aperture fields $f_B(x, y)$.
4) Based on the phase distribution of the solved aperture fields, the antenna geometry, and operating wavelength, the equivalent surface errors on M1, which is the sum

of errors on M1 and M2, can be computed, see Fig. 4 (right).

The main beam is obviously distorted. The inferred surface deformation in Fig. 4 right indicates all error patches, also points out the large spatial twist error in the antenna optics. But only using this error map cannot discriminate where the errors come from. These will be analyzed by following the 'Multi-map' holography.

B. Multi-map Holographic Analysis

The 'Multi-map' approach uses all five complex beam maps measured with the receiver at the five positions shown in Fig. 2. Fig. 5 displays the observed on-axis and four off-axis beam maps. The off-axis beams shift the projection of mirror errors in the aperture plane, allowing to separate the error contribution by their respective parallax. We can convert the five complex beams to two mirror surface maps using the numerical fitting algorithm described in paper [7], which expresses the surface errors by a set of parameters and find their values that can make the simulated beam best fit to the observed beam maps. We first research the error source of the twist-like errors in Fig. 4. The mirror surfaces of the small antenna are represented by Zernike polynomials [9] with maximum order of 7$^{\text{th}}$ (36 orthogonal polynomials). The fitting results shown in Fig. 6 top indicate that the twist-like errors come from M1.

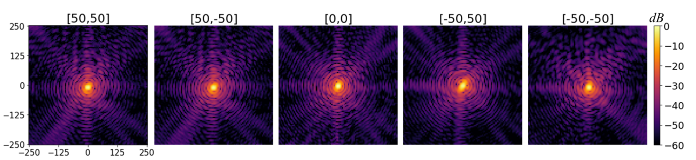

Fig. 5. The observed 5 distorted focused beams with the receiver located at positions [50mm,50mm], [50mm,-50mm], [0,0], [-50mm,50mm], and [-50mm,-50mm] relative to the center of the focal plane.

To find out the small artificial errors, more polynomials are required to achieve high spatial resolution, for example, employing a set of polynomials with maximum order of 30$^{\text{th}}$ (496 parameters on each mirror needed to be fitting), more details of the surface quality are resolved, see Fig. 6 bottom. All four artificial piston errors (3 patches on M1 and 1 copper foil on M2) are clearly detected in their correct location. The two plastic tape patches introduce a fraction of phase delay that is equivalent to negative piston panel errors. Their precise phase delay is not well known because of the multi-reflection between the two surfaces and the difficulty of attaching them tightly to the mirror surface.

The statistical error of the measurement can be studied by repeating the measurements, which shows a random variations of the surface with a RMS scatter of $< 1\,\mu$m.

The resolved surface errors in Fig. 6 show a twist-like error on M1. To verify this, the deformation of M1 was checked mechanically, and was found to be caused by misalignment of the mounting frame. Correcting this misalignment fixed the beam distortion. Fig. 7 shows the comparison of the beam affected by the twist error on M1 and the beam after error

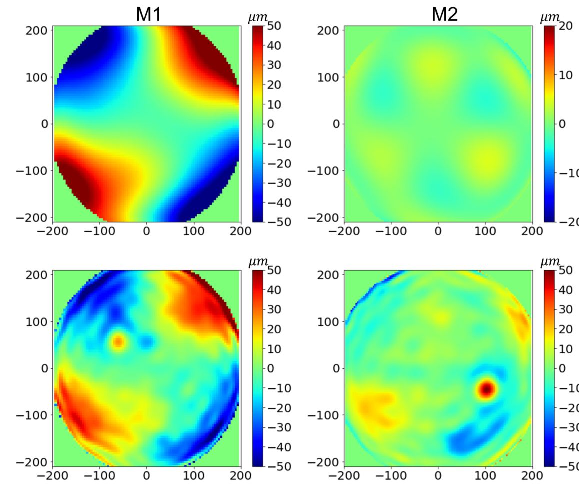

Fig. 6. The deduced surface errors analyzed by the 'Multi-map' holography algorithm. Top is the fitted surface errors only in large spatial scale using 36 Zernike polynomials with maximum order of 7$^{\text{th}}$ for each mirror surface. Bottom is the more detailed surfaces that are resolved by fitting 496 parameters per mirror (992 in total).

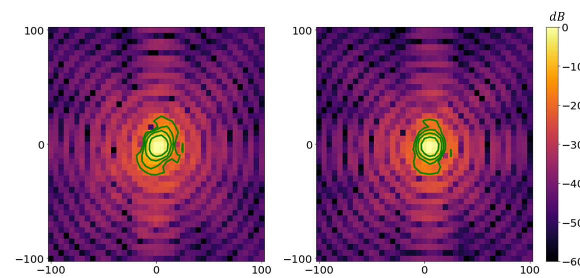

Fig. 7. Observed focused beam of the laboratory antenna. Left is the measured beam distorted by the twist error on M1; Right is the one after the large error was corrected. Blue curves are the contour map of the observed beam.

correction. This shows that the novel 'multi-map' holography technique can also correctly identify and discriminate the large-scale errors of the mirror surfaces.

IV. Conclusion

A near-field beam measurement system has been built to measure the surface profile of the two reflectors of the small version FYST antenna. The feasibility of the new 'Mutli-map' holographic technique is proven. Employing this technique, the small-scale surface deviations on the two reflectors can be measured and discriminated with a repeatable error less than $< 1\mu m$. The deformations in large spatial scale of the reflectors, such as errors caused by gravity and thermal expansions, can also be diagnosed. The experiments cannot check the accuracy of the measured large spatial errors because the laboratory antenna cannot be adjusted with predictable behavior. But we believe that repeating a couple of times of the holographic measurements and panel adjustments for the full-size FYST telescope can correct the large spatial errors.

Acknowledgments

The work is carried out at UniversitUniversität zu Köln and supported by the Colaborative Research Centre 956, subprojects D2 and S, and funded by the Deutsche Forschungsgemeinschaft (DFG)-project ID 184018867. The team at Universidad de Chile acknowledge the support from ANID through project QUIMAL 180004. We would like to dedicate this paper to the memory of Richards Hills.

REFERENCES

[1] J. Bennett, et al., "Microwave holographic metrology of large reflector antennas," in *IEEE Transactions on Antennas and Propagation*, vol. 24, no. 3, pp. 295-303, May 1976.
[2] Scott, P. F. and Ryle, M., "A rapid method for measuring the figure of a radio telescope reflector.", *Monthly Notices of the Royal Astronomical Society*, vol. 178, pp. 539–545, 1977.
[3] C. Dragone, "Offset multireflector antennas with perfect pattern symmetry and polarization discrimination," in *The Bell System Technical Journal*, vol. 57, no. 7, pp. 2663-2684, Sept. 1978.
[4] Niemack, M. D., "Designs for a large-aperture telescope to map the CMB 10X faster", Applied Optics, Vol. 56, No. 7, pp.1688-1696 (2016).
[5] Parshley, S. C., et al., "CCAT-prime: a novel telescope for sub-millimeter astronomy," Proc. SPIE 10700, Ground-based and Airborne Telescopes VII, 107005X (6 July 2018).
[6] Parshley, S. C., et al., "The optical design of the six-meter CCAT-prime and Simons Observatory telescopes," Proc. SPIE 10700, Ground-based and Airborne Telescopes VII, 1070041 (6 July 2018);
[7] Ren, X., et al., "Holographic surface measurement system for the Fred Young Submillimeter Telescope," Proc. SPIE 11445, Ground-based and Airborne Telescopes VIII, 114456D (13 December 2020)
[8] H. J. Gibson, et al., "A Novel Spline-Profile Diagonal Horn Suitable for Integration Into THz Split-Block Components," in IEEE Transactions on Terahertz Science and Technology, vol. 7, no. 6, pp. 657-663, Nov. 2017, doi: 10.1109/TTHZ.2017.2752423.
[9] Born, M. and Wolf, E., "Principles of Optics", Elsevier Science (1980).
[10] Goodman, J. W. 2005, Introduction to Fourier optics, 3rd ed., by J.W. Goodman. Englewood, CO: Roberts & Co. Publishers, 2005